Water Supply

IWA PUBLISHING

Water Supply Vol 24 No 3, 901 doi: 10.2166/ws.2024.047

An improved transfer coefficient method considering the combined effect of reservoir level variation and rainfall and its application in the stability evaluation of multistage sliding ancient landslides

Xiaofeng Gou[a], Mo Xu[a], Xiao Li[b], Anrun Li[a] and Hui Deng[a,*]

[a] State Key Laboratory of Geohazard Prevention and Geoenvironment Protection, Chengdu University of Technology, Chengdu 610059, China
[b] Tianfu Yongxing Laboratory, Chengdu 610200, China
*Corresponding author. E-mail: dh@cdut.edu.cn

ABSTRACT

In this paper, by considering the dynamic water pressure and particle migration effect caused by reservoir level variation, the weakening effect of slip zone soil influenced by rainfall infiltration, and the interaction force between multistage sliding bodies, an improved transfer coefficient method for multistage sliding ancient landslide is proposed under the combined action of reservoir level variation and rainfall. The results show that (1) the combined action of reservoir level variation and rainfall has a significant influence on the stability of multistage sliding ancient landslides. (2) The sliding force calculated by the improved transfer coefficient method is smaller than the calculation result by the traditional transfer coefficient method, and the residual sliding force is larger. The different sliding body stability coefficient is reduced by about 28.84, 18.13, 19.26, and 21.01%, respectively. (3) The stability results calculated by the traditional transfer coefficient are higher than the improved transfer coefficient method, which may lead to deviation in the multistage sliding ancient landslide stable state judgment. (4) This improved transfer coefficient method can provide a reference for the multistage sliding ancient landslides stability accurate evaluation in hydropower station reservoir area.

Key words: combined effect of reservoir level variation and rainfall, improved transfer coefficient method, multistage sliding ancient landslide, stability evaluation

HIGHLIGHTS

- For the landslide disaster risk management in hydropower station reservoir area, a new method of ancient landslide multistage landslide stability evaluation under the combined influence of water storage and rainfall is proposed.
- This improved transfer coefficient method considers the effect of particle migration caused by dynamic water pressure, the difference of strength parameters in slip zone different parts, and the influence of the interaction force between multistage sliding bodies.

GRAPHICAL ABSTRACT

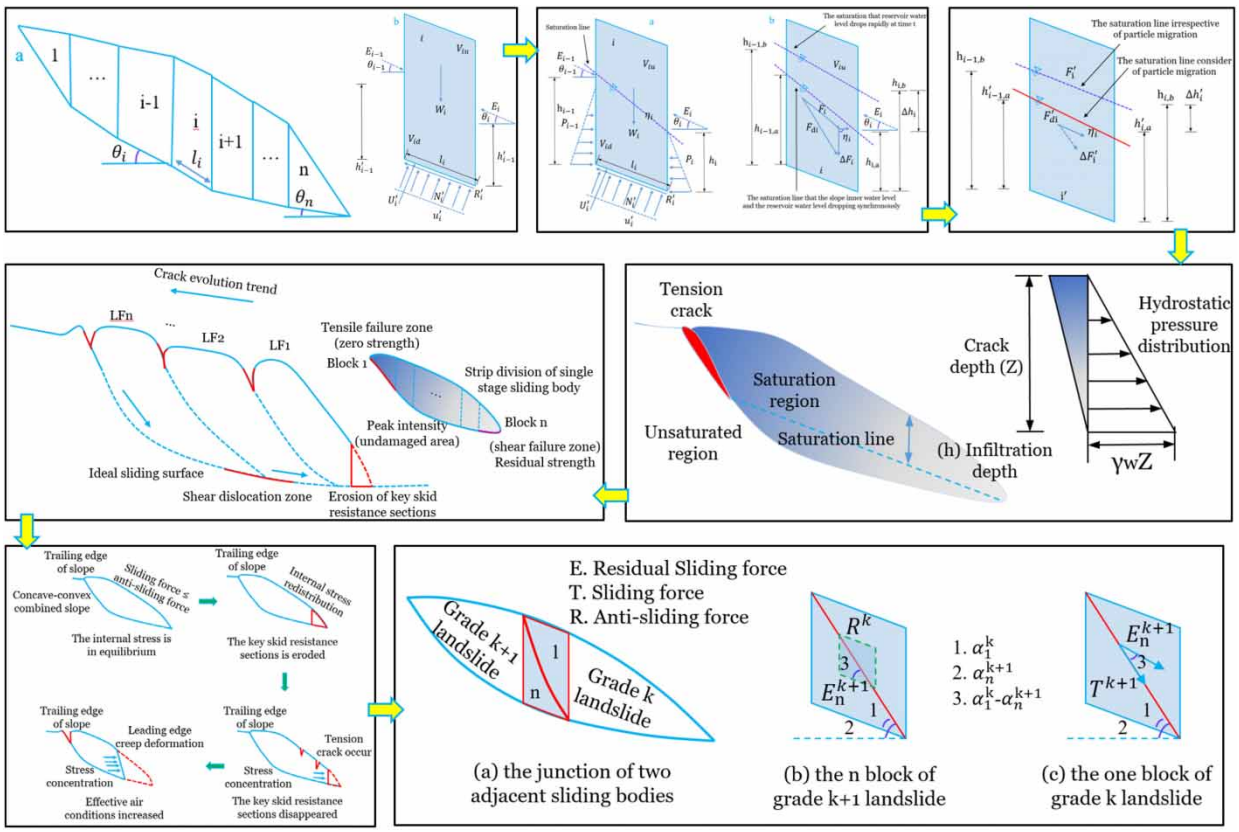

1. INTRODUCTION

With the water storage operation in the Three Gorges, Xiaowan, Baihetan, and other hydropower projects, affected by climate change and reservoir water level periodic fluctuation, the runoff will increase, and the erosion of ancient landslides will revive. The ancient landslide often shows the form of multistage sliding (Xu & Ma 1979; Shahid *et al.* 2018; Wang *et al.* 2020; Wen *et al.* 2022; Xu 2022). Multistage landslides usually refer to the same sliding pattern, repeated shows many times. The common instability process of multistage sliding is as follows: leading edge unloading induces the trailing edge to produce tractive multistage tension (Ren 2020; Guo *et al.* 2021; Jiang *et al.* 2022). In the reservoir area of a hydropower station, it is difficult to make a rapid and accurate evaluation of the ancient landslides' multistage sliding mechanism and stability due to the combined influence of reservoir water level variation, bank slope erosion, and rainfall (Haeri *et al.* 2021; Tong *et al.* 2021; Yang *et al.* 2022). Therefore, it is of great practical engineering significance to accurately evaluate the stability of multistage sliding ancient landslides under the combined effect of reservoir level variation and rainfall. An improved transfer coefficient method is necessary by considering the dynamic water pressure and particle migration effect caused by reservoir level variation, the weakening effect of slip zone soil influenced by rainfall infiltration, and the interaction force between multistage sliding bodies.

The main stability analysis methods of multistage sliding ancient landslides are as follows: (1) using numerical simulation software combined with strength reduction method to search the potential sliding surface of multistage landslides, respectively, and using the limit equilibrium method to calculate the stability (Xiao *et al.* 2013; Song *et al.* 2019). (2) Based on nonlinear theory, the Monte Carlo method and other statistical and probability theory methods were used to analyze the reliability of multistage landslides (He *et al.* 2011). (3) The limit equilibrium analysis method, based on the principle of static equilibrium, analyzes the stress state of a multistage landslide under different failure modes and determines the multistage landslide stability by analyzing the ratio relationship between landslide anti-sliding force and sliding force. Among them, the transfer coefficient method is a widely used limit equilibrium analysis method, which has the advantages of simple calculation principles and intuitive calculation processes (Tan *et al.* 2015; Pacheco *et al.* 2023; Zhao *et al.* 2023).

However, the current research shows that when the traditional transfer coefficient method is used to calculate the stability of ancient landslide under the multistage sliding mode, the influence of factors such as the combined effect of reservoir level variation and rainfall, complex sliding mode, and the difference of sliding zone soil parameters is not taken into account, the stability coefficient calculated results is often too large, resulting in insufficient design safety reserve of the retaining project (Wang *et al.* 2022; Xue *et al.* 2023; Yang *et al.* 2023). Many scholars have conducted improved studies on the transfer coefficient method, mainly focusing on (1) improving the transfer coefficient method based on the migration effect of slipping soil particles caused by seepage under dynamic water conditions (Ren 2020). (2) Improving the transfer coefficient method by considering the interaction force of sliding bodies and the different sliding surface dip angles at the bottom of sliding bodies (He & Zhao 2010). (3) Improving the landslide sliding force calculation formula by considering the interaction force of sliding bodies under the multistage sliding mode (Tan *et al.* 2016; Sarada & Tariq 2020). In summary, although many scholars have explored the transfer coefficient method for calculating the stability of ancient landslides and have achieved good results, most of them only consider the influence of single factors such as rainfall, earthquake, or reservoir water level change. It is still rare to study the transfer coefficient method of multistage sliding ancient landslide stability under the combined action of multiple factors such as rainfall and reservoir water level (Xu & Wang 1980; Chen *et al.* 2020; Li *et al.* 2022; Wu *et al.* 2022).

Therefore, the uniqueness of this manuscript compared with other literature is that the traditional transfer coefficient method is improved under the condition of reservoir level variation, the particle migration effect of the sliding body, the action of dynamic water pressure, the sliding zone soil parameter value obtained in the multistage sliding body progressive failure during rainfall infiltration, and the influence of the interaction between multistage sliding bodies. The research results are expected to provide a new reference for the stability accurate evaluation of multistage sliding ancient landslides under the combined action of reservoir level variation and rainfall in hydropower stations. The structure of this manuscript is arranged as follows: (1) the effect of particle migration caused by reservoir water level variation on landslide stability; the influence of dynamic water pressure caused by reservoir water level fluctuation on landslide stability; (2) an improved transfer coefficient method considering the combined effect of reservoir water level variation and rainfall is proposed; (3) calculation cases; the improved transfer coefficient method is compared with the traditional method.

2. IMPROVED TRANSFER COEFFICIENT METHOD CONSIDERING PARTICLE MIGRATION EFFECT UNDER RESERVOIR WATER LEVEL VARIATION

2.1. Calculation of stability coefficient by traditional transfer coefficient method

The transfer coefficient method was proposed by Xu & Ma (1979), which is mainly applicable to the stability calculation of broken lines slope form. In practical engineering, the width of sliding bodies is divided into small enough. The sliding surface of different sliding bodies can be approximately regarded as a straight line. The transfer coefficient method can be used for analysis of this slope stability. At the same time, since the transfer coefficient method is an explicit solution process when solving the stability coefficient, it is widely used in engineering practice (Figure 1). The bottom supporting force N_i of the sliding body is as follows:

$$N_i = W_i \cos\theta_i - U_i + E_{i-1} \sin(\theta_{i-1} - \theta_i) \tag{1}$$

In the direction of the strip bottom, the resultant force is:

$$W_i \sin\theta_i = R_i - E_{i-1} \cos(\theta_{i-1} - \theta_i) + E \tag{2}$$

Therefore, according to the static equilibrium condition, the calculation formula of the force E_i between strips can be obtained as follows:

$$E_i = W_i \sin\theta_i - c_i l_i + (W_i \cos\theta_i - U_i) \tan\varphi_i + E_{i-1}\psi_{i-1} \tag{3}$$

Stability coefficient is calculated by the traditional transfer coefficient method.

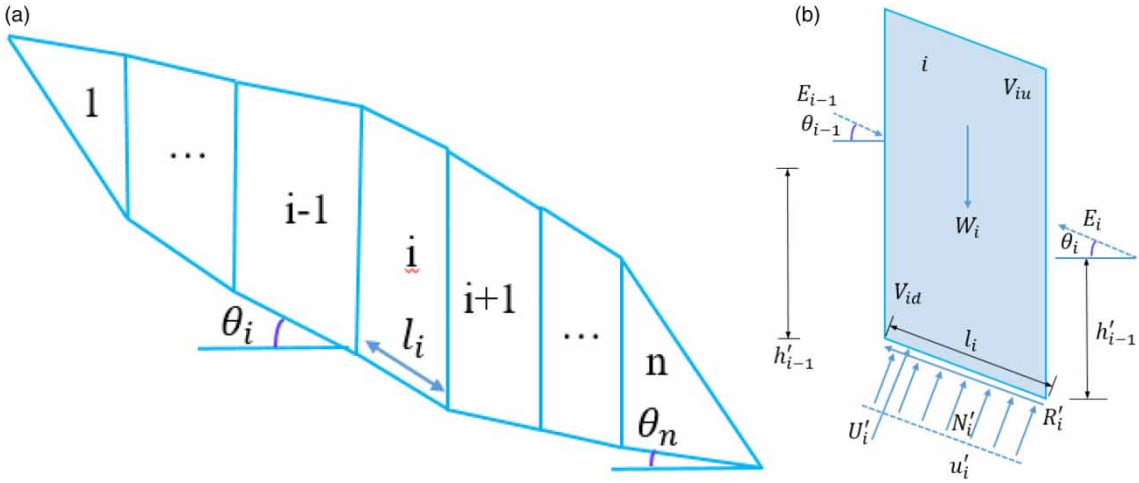

Figure 1 | Calculation diagram of traditional transfer coefficient method ((a) sliding bodies division diagram; (b) strip force analysis).

ψ is the transfer coefficient, and its specific expression is as follows:

$$\psi_{i-1} = \cos(\theta_{i-1} - \theta_i) - \tan\varphi_i \sin(\theta_{i-1} - \theta_i) \tag{4}$$

Formula 4 can be simplified to formula 5 as follows:

$$E_i = T_i - R_i + E_{i-1}\psi_{i-1} \tag{5}$$

where T is the sliding force and R is the anti-sliding force. The calculation formulas are as follows:

$$T_i = W_i \sin\theta_i \tag{6}$$

$$R_i = c_i' l_i + N_i \times \tan\varphi_i' \tag{7}$$

It can be seen that the last strip has the following expression:

$$E_n = \left(T_n + \sum_{i=1}^{n-1} T_i \prod_{j=1}^{n-1} \psi_j\right) - \frac{1}{F_s}\left(R_n + \sum_{i=1}^{n-1} R_i \prod_{j=1}^{n-1} \psi_j\right) \tag{8}$$

Let $E_n = 0$, then the formula for landslide stability coefficient calculation can be obtained:

$$F_s = \frac{R_n + \sum_{i=1}^{n-1} R_i \prod_{j=1}^{n-1} \psi_j}{T_n + \sum_{i=1}^{n-1} T_i \prod_{j=1}^{n-1} \psi_j} \tag{9}$$

2.2. Calculation of stability coefficient affected by dynamic water pressure actions under reservoir water level variation conditions

The stability of ancient landslides in reservoir areas is significantly different because of the reservoir water level variation conditions. Therefore, the transfer coefficient method based on traditional hydrostatic pressure conditions has different expressions in soil-water combined calculation and soil-water separated calculation. The traditional transfer coefficient method is improved by considering the action of dynamic water pressure. The improving methods are more suitable for accurate calculation of the stability coefficient under dynamic water pressure (Figure 2).

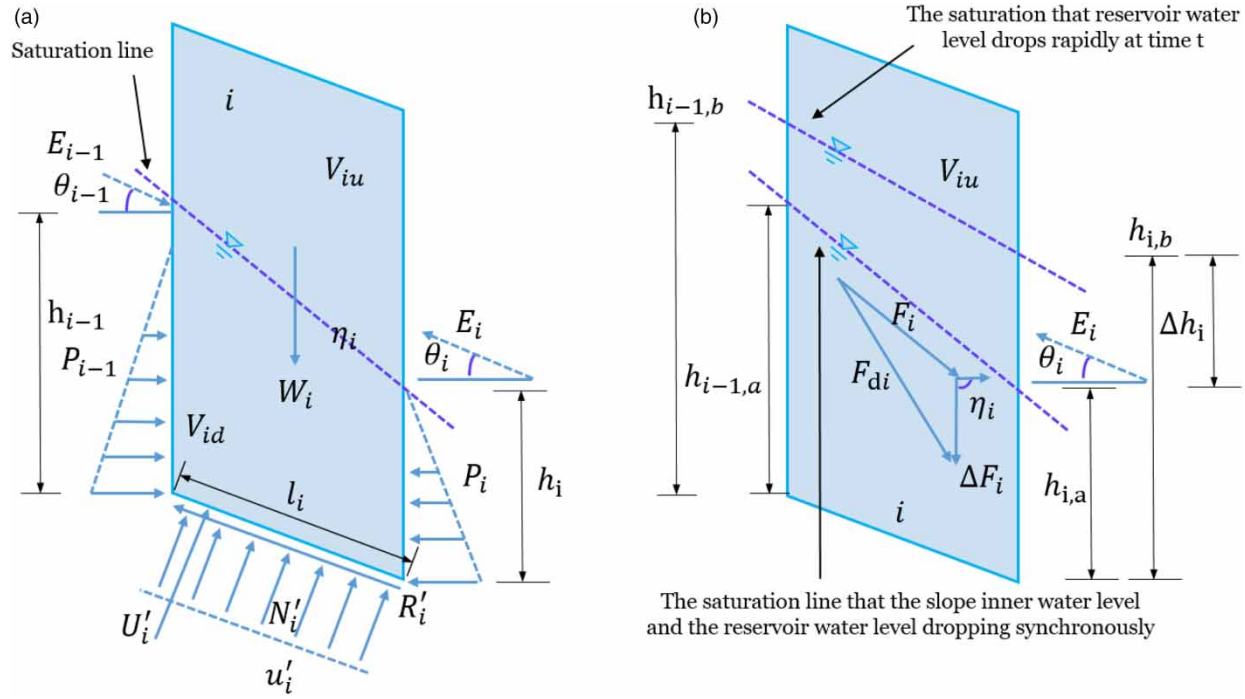

Figure 2 | Calculation diagram of transfer coefficient method under dynamic water pressure caused by reservoir water level variation ((a) only the saturation line is considered; (b) consider the influence of reservoir water level variation).

As shown in Figure 2(a), when calculating the stability coefficient of the saturation part of the landslide, the supporting force N_i at the bottom of the strip is:

$$N_i = W_i \cos\theta_i - U_i - (P_{i-1} - P_i)\sin\theta_i + E_{i-1}\sin(\theta_{i-1} - \theta_i) \tag{10}$$

Similarly, in the direction along the strip bottom, there are:

$$R_i = c_i l_i + (W_i \cos\theta_i - U_i + (P_{i-1} - P_i)\sin\theta_i)\tan\varphi_i \tag{11}$$

$$W_i \cos\theta_i - (P_{i-1} - P_i)\cos\theta_i = R_i - E_{i-1}\cos(\theta_{i-1} - \theta_i) + E_i \tag{12}$$

where P_i is the hydrostatic pressure on the strip i, and its specific calculation formula is as follows:

$$P_i = \frac{1}{2}\gamma_w h_i^2 \tag{13}$$

where γ_w is the water weight, and the water level height on the contact line between strip i and strip $i+1$.

With the study result of Zhang (2019), which considers the influence of hydrodynamic pressure on the calculation of the bank slope stability coefficient, the calculation of the ancient landslide stability coefficient under reservoir level variation is analyzed as follows. The dynamic water pressure is caused by the small infiltration coefficient of the sliding body and the dissipation of pore water pressure in the sliding body inner behind the decrease of osmotic force under the reservoir water level variation conditions. When the water level in the sliding body inner decreases simultaneously with the reservoir water level, the sliding body is affected by the stable osmotic force F_{dit} (Figure 2(b)). At the time t, when the reservoir water level rises and drops rapidly, after the pore water pressure dissipation in the sliding body inner, the seepage pressure is F_{it}.

When the reservoir water level drops rapidly, compared with the water level in the i strip when the reservoir water level is synchronized, a water level difference Δh_i will be formed, and resulting in a dynamic water pressure ΔF_i. The dynamic water

pressure ΔF_i is the vector difference between the osmotic force F_{it} when the reservoir water level drops and the stable osmotic force F_{dit} when the strip water level and the reservoir water level decrease synchronously, that is: $\overline{\Delta F_i} = \overline{F_i} - \overline{F_{di,a}}$.

When the width of the strip is small enough, the saturation line inside the strip can be approximately regarded as a straight line. When the dynamic water pressure gradient Δi_i is calculated, the water level difference Δh_i is obtained by the average value between the water level difference inside the i strip in the condition of the two states of reservoir water level synchronous reduction of slope water level and rapid reduction of reservoir water level. That is the height difference between the strip's two infiltration lines midpoints. The specific functions are expressed as follows.

$$\Delta i_i = \frac{\Delta h_i}{l_i \cos \theta_i} = \frac{(h_{i-1,b} - h_{i,b}) - (h_{i-1,a} - h_{i,a})}{2 l_i \cos \theta_i} \tag{14}$$

Therefore, the calculation formula under dynamic water pressure conditions can be obtained as follows.

$$\Delta F_i = \gamma_w \cdot \Delta i_i \cdot V_{id} \tag{15}$$

As shown in Figure 2(b), the angle between the dynamic water pressure and the horizontal direction is η_i. The specific expression of the supporting force N_i at the bottom of the strip can be rewritten as follows.

$$N_i = W_i \cos \theta_i - U_i + (P_{i-1} - P_i) \sin \theta_i + \Delta F_i \sin (\eta_i - \theta_i) + E_{i-1} \sin (\theta_{i-1} - \theta_i) \tag{16}$$

Similarly, the calculation formula of T_i and R_i can be changed as follows.

$$T_i = W_i \cos \theta_i + P_{i-1} \cos \theta_i - P_i \cos \theta_i + \Delta F_i \cos (\eta_i - \theta_i) \tag{17}$$

$$R_i = c_i l_i + (W_i \cos \theta_i - U_i + (P_{i-1} - P_i) \sin \theta_i) + \Delta F_i \sin (\eta_i - \theta_i) + E_{i-1} \sin (\theta_{i-1} - \theta_i) \tag{18}$$

The transfer coefficient formula is the same as that of Equation (8). By substituting Equations (16)–(18) into the inter-strip force Equation (8), the stability coefficient calculation formula of the ancient landslide saturated part under the condition of dynamic water pressure effects can be derived by making $E_n = 0$.

2.3. Calculation of stability coefficient affected by particle migration actions under reservoir water level variation conditions

In the process of ancient landslide stability coefficient calculating under the condition of reservoir water variation, the particle migration process is shown in Figure 3.

Considering the influence of particle migration, the change of landslide body infiltration coefficient, and the change of saturation line inside the landslide, the action of hydrodynamic pressure on the landslide body is calculated and corrected as follows (Figure 4).

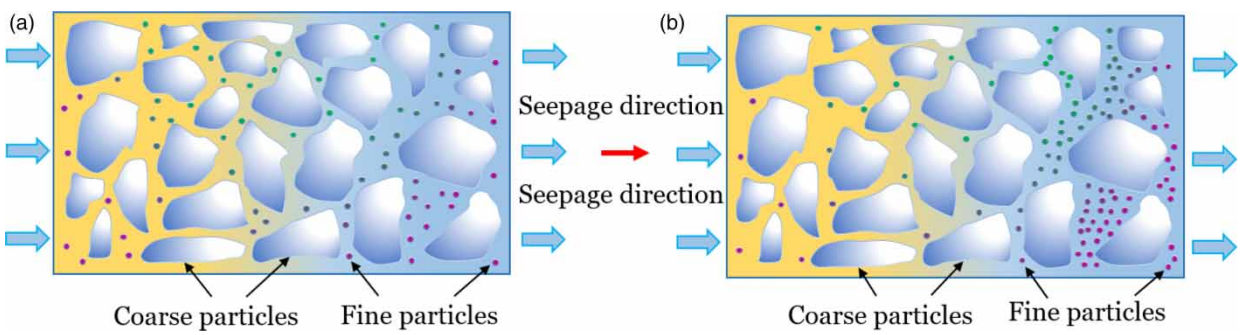

Figure 3 | The particle migration process affected by reservoir water variation inside the multistage sliding ancient landslide ((a) particles migrated along the seepage direction; (b) fine particle enrichment).

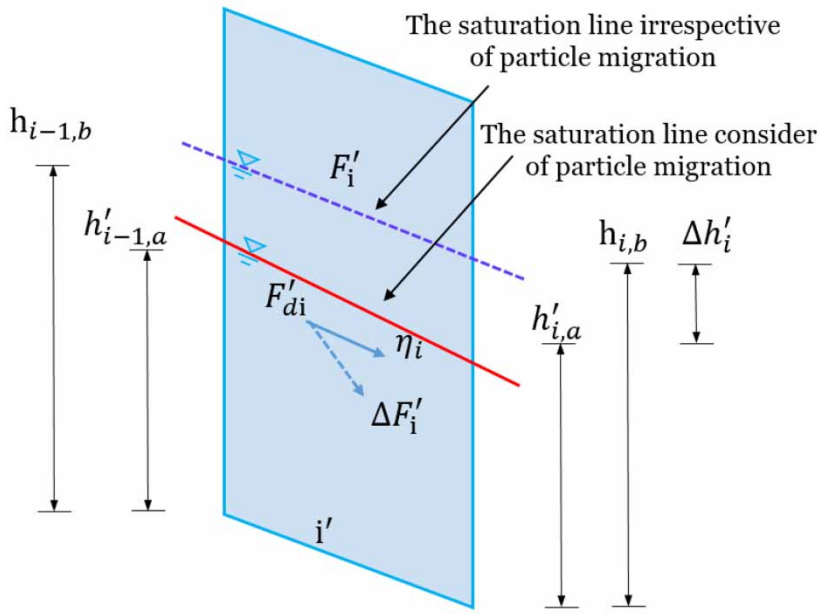

Figure 4 | Calculation diagram of transfer coefficient method of ancient landslide considering the particle migration caused by reservoir water level variation.

The dynamic water pressure calculation and improvement of the landslide-saturated part are as follows.

$$\Delta i_i^{'} = \frac{\Delta h_i^{'}}{l_i \cos\theta_i} = \frac{(h_{i-1,b}^{'} - h_{i,b}) - (h_{i-1,a}^{'} - h_{i,a})}{2l_i \cos\theta_i} \tag{19}$$

$$\Delta F_i^{'} = \gamma_w \cdot \Delta i_i^{'} \cdot V_{id} \tag{20}$$

The formula for sliding force and anti-sliding force is as follows.

$$T_i^{'} = W_i \sin\theta_i + P_{i-1}^{'} \cos\theta_i - P_i^{'} \cos\theta_i + \Delta F_i^{'} \cos(\eta_i - \theta_i) \tag{21}$$

$$R_i^{'} = c_i l_i + (W_i \cos\theta_i - U_i^{'} + (P_{i-1}^{'} - P_i^{'}) \sin\theta_i + \Delta F_i^{'} \sin(\eta_i - \theta_i) + E_{i-1} \sin(\theta_{i-1} - \theta_i)) \tag{22}$$

By substituting the improved sliding force and anti-sliding force into Equation (9), the stability coefficient of ancient landslides affected by particle migration can be obtained.

3. IMPROVED TRANSFER COEFFICIENT METHOD OF MULTISTAGE SLIDING ANCIENT LANDSLIDE UNDER THE COMBINED ACTION OF RESERVOIR LEVEL VARIATION AND RAINFALL

3.1. Multistage sliding mechanism of ancient landslide under the combined action of reservoir level variation and rainfall

Under the combined action of reservoir level variation and rainfall, the erosion effect of the ancient landslide front caused by the reservoir water level repeated rise and fall. And a multistage sliding phenomenon occurs (Song *et al.* 2019; Dolojan *et al.* 2023). Multistage tension cracks appear on the surface of the ancient landslide, which provide a preferential migration passage for rainwater to accelerate the landslide infiltration (Yi *et al.* 2023). At the same time, with the tension crack as the dividing line, the original landslide body is divided into multistage slide bodies, forming an obviously step placement (Sepe *et al.* 2023).

The combined effects of reservoir level variation and rainfall on ancient landslides are as follows: softening effect of sliding body and sliding zone soil and coupling effect of dynamic water pressure and hydrostatic pressure. Rainfall can significantly

reduce the physical and mechanical properties of the landslide body (Li *et al.* 2023; Sun *et al.* 2023), thus reducing the anti-sliding force of the landslide body. Meanwhile, the hydrostatic pressure at the crack and the dynamic water pressure at the front of the landslide body will further increase the sliding force (Figure 5).

When the rainfall intensity exceeds the infiltration capacity of the slope soil, the landslide soil surface will generate surface runoff. And the surface of the ancient landslide will reach a saturated state soon. Under the action of surface runoff, the cracks on the landslide surface develop rapidly and cause rainwater to quickly enter into the landslide inner. Due to the erosion effect of surface runoff, the landslide shape and structure will change, and the influence of reservoir water level rising and falling repeatedly will eventually cause the landslide body to produce multistage instability failure.

Along with the rainfall infiltration and the repeated rise and fall of reservoir water level, the region passed by the infiltration front and infiltration surface will reach the saturation state quickly. The mechanical parameters of the landslide body decrease rapidly and the stability coefficient decreases continuously. One of the key factors determining the multistage sliding ancient landslides instability is the sliding zone soil mechanical parameters (Liao *et al.* 2023). When the infiltration front and the infiltration surface reach the slip surface, the slip zone soil's physical and mechanical parameters will plummet in a short time. In this paper, it is considered that multistage sliding failure occurs when the infiltration front and the infiltration surface reach the sliding surface, and the parameters of the landslide are all saturated.

3.2. Parameter values obtained from sliding zone soil under the combined action of reservoir level variation and rainfall

Under the combined influence of reservoir level fluctuations and rainfall, the progressive failure process of ancient landslides in multiple stages is observed, with the soil mechanical properties within the slip zone gradually deteriorating (Liu *et al.* 2023). The soil strength parameters of the slip zone undergo a sequence of stages, including pre-peak stress, softening stress, and residual stress (Dou *et al.* 2023; Zhang *et al.* 2023a). In this study, when a tensile failure occurs at the upper portion of the multistage sliding body and shear failure transpires at the base of the slope, it is considered that the soil strength parameters within the sliding zone represent residual strength. Conversely, if the sliding surface of the ancient landslide is not connected and no apparent damage is observed in the middle section, the soil strength parameters within the sliding zone can be interpreted as peak stress. Throughout the multistage sliding process of ancient landslides, the downward extension of tensile failure from the slope's top synchronously develops with the upward extension of shear failure from the foot of the slope (Wang *et al.* 2023; Zhang *et al.* 2023b).

In the progressive failure process, the single sliding body is divided into three regions: Region 1, located at the upper left of the sliding body, is the tension failure zone, where the development of tension cracks causes the sliding body to break, and shear slide occurs along the fracture plane. Due to the occurrence of macroscopic fracture, the strength parameter of the sliding body in this region is considered to be zero. Region 2: located in the middle of the sliding body, is the critical undamaged region, and it is considered that the cohesion and internal friction angle of the sliding body in this region are both peak values. Region 3: located at the lower right, is the shear failure zone. Obvious shear failure occurs in the sliding body in this region. It is considered that the cohesive force and internal friction angle values of the sliding body in this region are residual values.

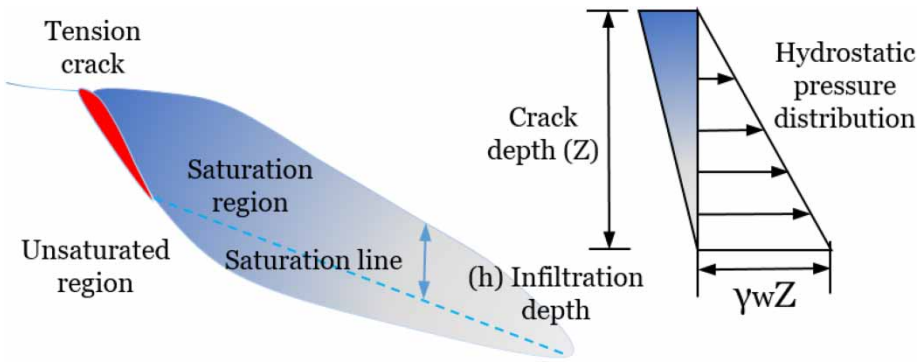

Figure 5 | The hydrostatic pressure schematic diagram of a single sliding body trailing edge tensile crack.

With the repeated variation of reservoir water level and the continuous rainfall infiltration effect, the ancient landslide further deformed, and the tension failure zone and shear failure zone gradually expanded to the critical undamaged zone in the middle. Finally, the sliding body was in a state of failure. The tension failure zone and shear failure zone were connected, forming a multi-level sliding body (Figure 6).

3.3. Interaction force between multistage sliding bodies under the combined action of reservoir level variation and rainfall

Under the combined action of reservoir level variation and rainfall, the interaction force between multistage sliding bodies of the ancient landslides has a great influence on the stability coefficient calculation result. By analyzing the progressive failure process, it can be seen that the ancient landslide multistage slide failure is repeated by multiple secondary landslides sliding with the same failure mode. The back sliding body will slide when the first-stage slide body fails, because the front of the key strip anti-sliding force decreases or even disappears. Therefore, it can be considered that the interaction force of different stripes has a significant influence on the multistage sliding ancient landslides (Figure 7).

Taking the two strips interaction force at the junction of two adjacent sliding bodies as an example analysis, the stress process is simplified as shown in Figure 8, in which the position relationship between the first strip of the k-stage sliding body and the last strip of the k + 1 stage sliding body is shown in Figure 8(a). When the interaction force on the junction of two adjacent landslides is the residual sliding force of the k + 1 stage sliding body last strip, the resistance of the k-stage sliding body to the k + 1 stage sliding body should be greater than or equal to the force absolute value. For the convenience of calculation, it is assumed that the k-stage sliding body is in a critical state. The k + 1 stage sliding body has shown an obvious downward sliding trend. The back-stage sliding body has a certain thrust effect on the pre-stage sliding body. The residual sliding force of the back-stage sliding body's last strip will be transmitted downward in the form of thrust.

3.4. Improved transfer coefficient method of ancient landslide under the combined action of reservoir level variation and rainfall

Considering the difference of strength mechanical parameters in the ancient landslide multistage sliding body progressive failure process, the interaction force between strip and block, and the dynamic and hydrostatic water pressure under the combined action of reservoir water level variation and rainfall, the traditional transfer coefficient method is improved. According to *the specific* division of the k ($k = 1,2,3,\ldots,m$) *stage* sliding body failure region, the calculation formula of residual sliding force is improved accordingly, which are as follows.

$$\begin{cases} E_i^k = W_i^k \sin\alpha_i^k - W_i^k \cos\alpha_i^k \tan\varphi_i^{k_{\text{resid}}} - c_i^{k_{\text{resid}}} l_i^k + \psi_i^k E_{i-1}^k - \dfrac{1}{2}\gamma_w Z^2, & i = 1 \\ E_i^k = W_i^k \sin\alpha_i^k - W_i^k \cos\alpha_i^k \tan\varphi_i^{k_{\text{peak}}} - c_i^{k_{\text{peak}}} l_i^k + \psi_i^k E_{i-1}^k, & 2 \le i \le n-1 \\ E_i^k = W_i^k \sin\alpha_i^k - W_i^k \cos\alpha_i^k \tan\varphi_i^{k_{\text{resid}}} - c_i^{k_{\text{resid}}} l_i^k + \psi_i^k E_{i-1}^k, & i = n \end{cases} \tag{23}$$

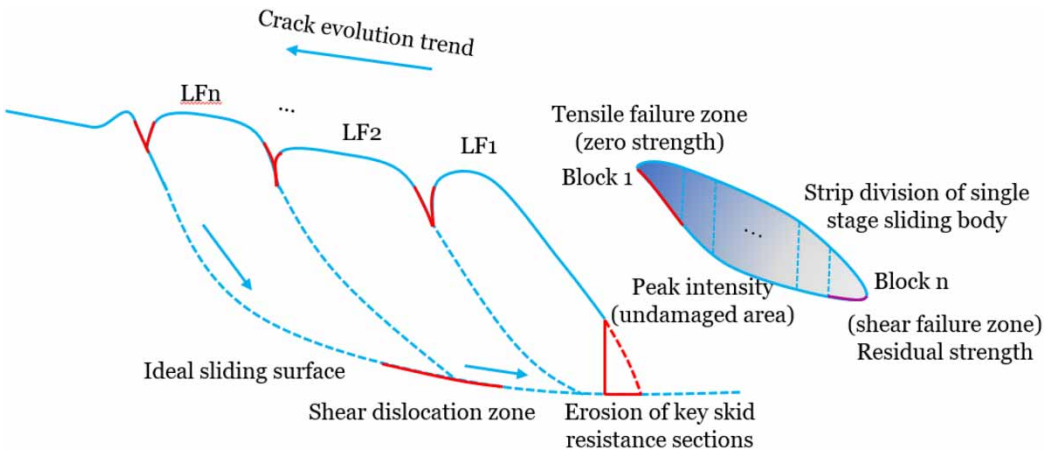

Figure 6 | Sliding zone soil parameters region dividing of multistage sliding ancient landslides under the combined effect of reservoir level variation and rainfall.

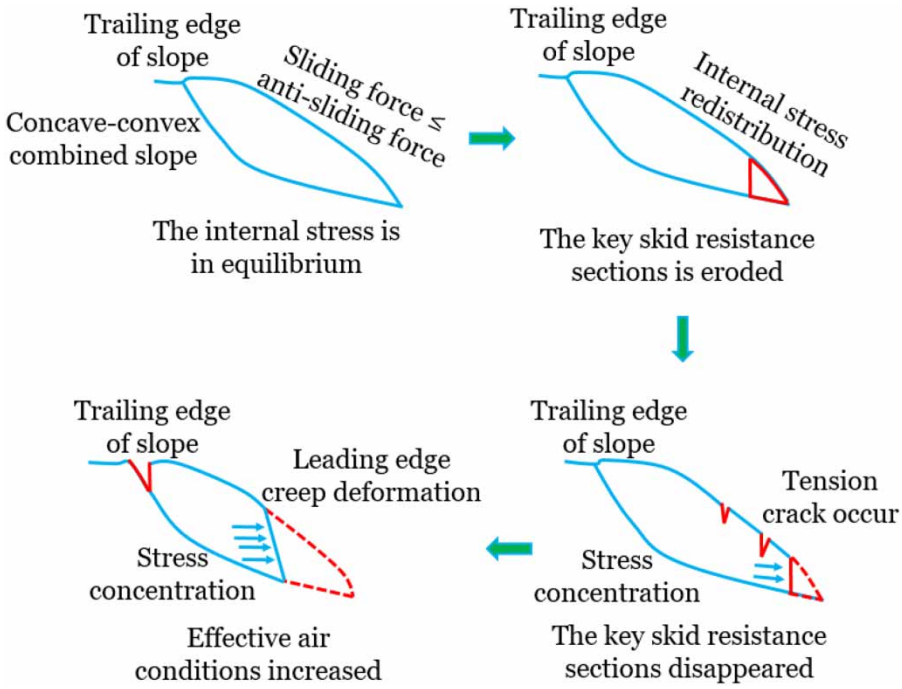

Figure 7 | The single-stage sliding body progressive instability process in multistage sliding ancient landslides.

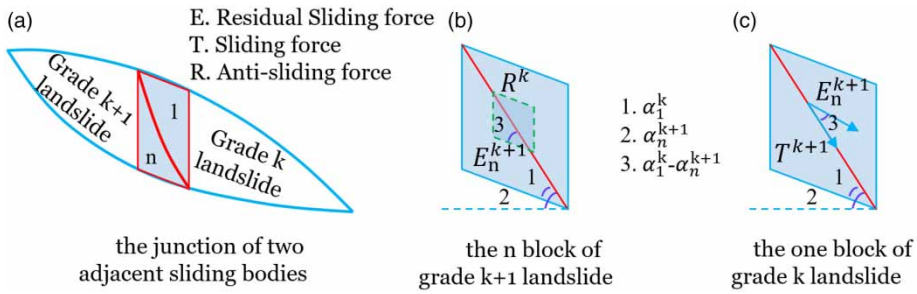

Figure 8 | Diagram of secondary landslides interaction force analysis under ancient landslides multistage slide ((a) schematic diagram of the interface of multistage slide bodies; (b) force analysis of the $k+1$ stage sliding body and the n strip; (c) force analysis of the k-stage sliding body and the first strip).

where W_i^k is the gravity of the i strip of k-stage sliding body. ψ_i^k is the transfer coefficient of the i strip of k-stage sliding body. α_i^k is the inclination angle of the i strip of k-stage sliding body. E_i^k is the residual sliding force of the i strip of k-stage sliding body. E_{i-1} is the residual sliding force of the $i-1$ strip. $c_i^{k_{\text{peak}}}$, $\varphi_i^{k_{\text{peak}}}$ are the peak strength parameters of the corresponding slide strip. $c_i^{k_{\text{resid}}}$, $\varphi_i^{k_{\text{resid}}}$ are the residual strength parameters of the corresponding slide strip. Z is the tensile crack depth. γ_w is the volume weight of water. l_i^k is the length of the i strip in the k-stage sliding body failure region.

The transfer coefficient is calculated as follows.

$$\psi_i = \cos(\alpha_{i-1} - \alpha_i) - \sin(\alpha_{i-1} - \alpha_i)\tan\varphi_i \tag{24}$$

where when $2 \le i \le n-1$, $\varphi_i = \varphi^{\text{peak}}$; when $i = n$, $\varphi_i = \varphi^{\text{resid}}$.

Where, the tensile crack depth $Z = 2c/\gamma\sqrt{K_a}$, $K_a = \tan^2(45^\circ - \varphi/2)$. Here, c and φ are the corresponding residual strength values.

According to the calculation of the multistage sliding body residual sliding force, it can be known that when the sliding body is in a critical state, the anti-sliding force of the strip is equal to the sliding force, and $E_n = 0$. When the sliding force

of the strip is greater than the anti-sliding force, the sliding body is in an unstable state, and $E_n > 0$. When the sliding force of the strip is less than the anti-sliding force, the sliding body is in a stable state, and $E_n < 0$. For slope bodies in different states, the stability coefficient F_s can be characterized by a linear equation, but the interaction force between multistage slide bodies cannot be ignored.

Therefore, based on the derived formula of Wen and Zheng (John *et al.* 2016; Wen *et al.* 2022; Zhang *et al.* 2023c), the following improvements are made in this paper: (1) when calculating the stability of the first-stage sliding body, and in the process of the anti-sliding force calculation, due to the erosion of the sliding body front edge caused by the reservoir water level repeated rise and fall should be subtracted. When calculating the sliding force, the thrust action of the rear sliding body should be considered. (2) When calculating the rear stage sliding body stability, the anti-sliding force calculation should take into account the absence of the previous stage sliding body. The calculation of the sliding force should take into account the post-stage sliding body anti-sliding force effect. When the ancient landslide has an m-stage sliding body, the stability coefficient calculation formula is as follows.

$$\begin{cases} F_s^k = \dfrac{\sum_{i=1}^{n-1}\left(R_i^k \prod_{j=i}^{n-1}\psi_i^k\right) + R_n^k - |R^o|}{\sum_{i=1}^{n-1}\left(T_i^k \prod_{j=i}^{n-1}\psi_i^k\right) + T_n^k + T^{k+1}}, & k = 1 \\ F_s^k = \dfrac{\sum_{i=1}^{n-1}\left(R_i^k \prod_{j=i}^{n-1}\psi_i^k\right) + R_n^k - |R^{k-1}|}{\sum_{i=1}^{n-1}\left(T_i^k \prod_{j=i}^{n-1}\psi_i^k\right) + T_n^k + T^{k+1}}, & k = 2, 3, L, \ldots, m-1 \end{cases} \tag{25}$$

Among them:

$$\begin{cases} T_i = W_i \sin\alpha_i, & i \neq n \\ T_i = W_i \sin\alpha_i + \dfrac{1}{2}\gamma_w Z^2, & i = n \end{cases} \tag{26}$$

$$R_i = W_i \cos\alpha_i \tan\varphi_i + c_i l_i \tag{27}$$

where R_i^{k-1} is the anti-sliding force of the $k-1$ stage on the k-stage sliding body. R^0 is the sliding starting force of the first-stage sliding body (the variation of reservoir water level leads to the slope leading edge erosion and a free surface emergence). l_i is the length of the i strip. T^{k+1} is the thrust force of the $k+1$ stage on the k stage sliding body. The specific formula is as follows.

$$T^{k+1} = \cos(\alpha_1^k - \alpha_n^{k+1})E_n^{k+1}, \quad k \geq 1 \tag{28}$$

$$R^{k-1} = -E_n^k \tag{29}$$

The multistage landslide sliding surface is formed from the beginning to the end. Therefore, the last stage is the k-stage sliding body, and it moves forward to the first-stage sliding body in turn.

4. CALCULATION EXAMPLE

4.1. Engineering geological conditions of T22 multistage sliding ancient landslide

The T22 multistage sliding ancient landslide of Xiaowan Hydropower Station is located in the Xiaowan Hydropower Station region in Lancang River. The main composition of landslide deposits is loessial powder soil and clay. The gravel content is 10%. The block diameter is 3–8 cm and the block diameter larger than 10 cm is rare. The bedrock is mainly the upper Jurassic purplish red mudstone and sandy mudstone with siltstone.

The trailing edge of the landslide body has an armchair shape on the terrain, forming a three-stage landslide platform from top to bottom. The first-stage platform is an ancient landslide subsidence zone with a width of nearly 100 m and a slope angle of 20°, and there are no new tension and collapse features. The width of the secondary platform is 20–30 m. The subsidence

zone has not been filled, and there is no new tensile deformation phenomenon. The surface dropping of the primary platform is 7–15 m. The rear edge steep wall is a secondary landslide wall, the color of the wall is dark after weathering, and weeds are crowded, indicating that there has been an obvious deformation phenomenon recently. The width of the three-stage platform is 5–9 m, with a slope angle of 25°–30°. The step main wall is 1–2 m high. Several 5–10 cm wide annular tension cracks and longitudinal tension cracks are developed. The length of annular cracks is 1–6 cm. Below the three-stage platform is a recent landslide. The front of this landslide is erosion. The collapse height caused by erosion is about 9 m, the transverse width is 26 m, the thickness is 4–6 m, and the estimated volume is 1,235 m^3 (Figure 9).

4.2. T22 multistage sliding ancient landslide deformation mechanism

The T22 multistage sliding ancient landslide is located in the Heihuijiang reservoir area of Xiaowan Hydropower Station in Lancang River. The geological structure is loose, and the stratigraphic lithology is Jurassic purplish red mudstone and sandy mudstone, which is easy to soften and has slipped before the water storage of Xiaowan Hydropower Station. With the impounded water of Xiaowan Hydropower Station, due to the influence of periodic reservoir water level rise and fall, its front suffers the influence of erosion, which leads to the loss of a key strip of the ancient landslide in front.

The phenomenon of multistage pulling cracks is shown. And the ancient landslide reactivation. In addition, under the influence of continuous heavy rainfall, rainwater develops infiltration from the loose quaternary deposits and vertical cracks at the top of the ancient landslide. Due to the sliding zone region being a relatively closed environment, after rainwater infiltration, the sliding zone soil is saturated. The mechanical strength is significantly reduced, and the saturated gravity of the slide body is increased, resulting in the sliding force increasing. Combined with the reservoir water erosion of the front, the anti-sliding force decreases, which intensifies the ancient landslide deformation, and the sliding surfaces are gradually connected forming a multistage sliding body.

The topographic features of the T22 ancient landslide reflect the spatial position relationship of each sliding body. The multistage sliding body occurs shear slip at the slope foot of the front primary sliding body, which is from the front to the back edge along the same main sliding direction and from the high-steep air face. The key slide strip at the slope foot is eroded by the reservoir water level variation. The sliding body strength decreases sharply. The front slope body preferentially forms tension cracks and becomes unstable, which provides a favorable slip space for the rear slide body downward sliding. Then the ancient landslide gradually failed and formed a multistage sliding body.

According to the failure characteristics of the T22 ancient landslide, it can be seen that the special geological conditions such as the development of cracks on the slope surface, the uneven slope surface, the loose and broken slope body, and

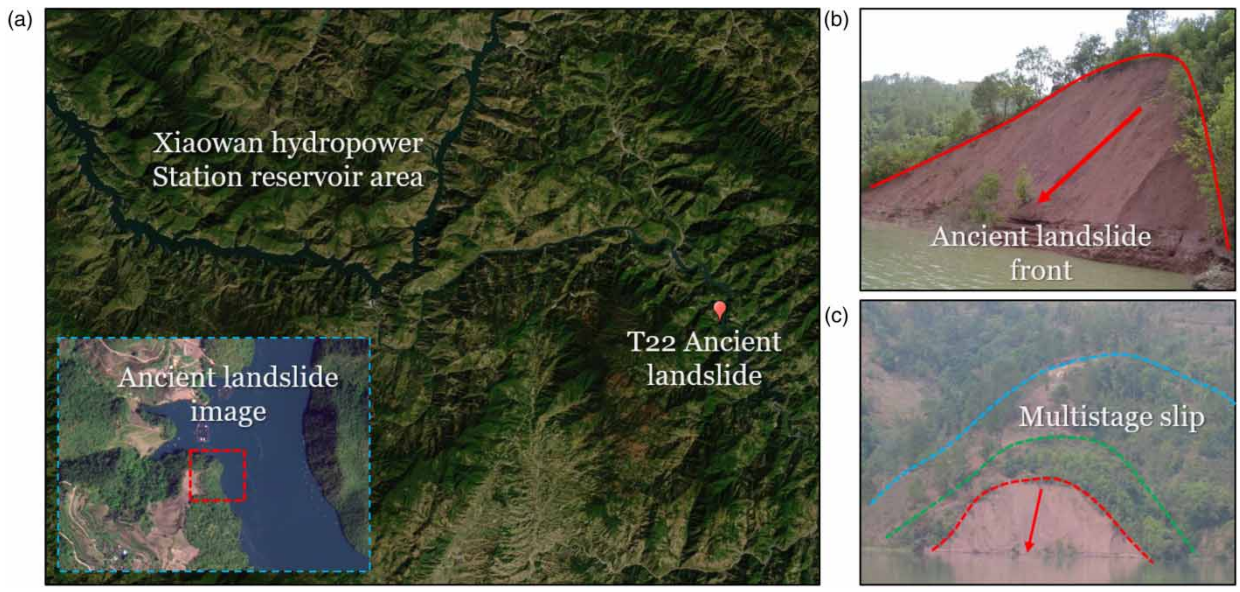

Figure 9 | T22 multistage sliding ancient landslide in Xiaowan Hydropower Station ((a) Xiaowan Hydropower Station reservoir remote-sensing image; (b) T22 ancient landslide front; (c) T22 ancient landslide multistage sliding characteristics).

the combination structure of soft and hard rock are the ancient landslide multistage sliding precondition. The combined effect of reservoir level variation and rainfall factors is the main external influencing factor for ancient landslide multistage sliding (Figure 10).

4.3. Selection of T22 multistage sliding ancient landslide sliding zone soil parameters

The slip zone soil saturated bulk density of the T22 multistage sliding ancient landslide in Xiaowan Hydropower Station is 21.2 kN/m^3. The partial strength parameters of the sliding zone soil obtained through laboratory tests are shown in Table 1.

To facilitate calculation, considering the reservoir water level repeated rise and fall and rainfall combined effect of the T22 multistage sliding ancient landslide in Xiaowan Hydropower Station, the saturation line is default reaches the slip surface. That is the region of the sliding body above the sliding surface reaches a saturation state. The T22 multistage sliding ancient landslide model is simplified. The specific strip division is shown as follows (Figure 11). According to the above analysis results on the interaction mechanism between sliding bodies of multistage sliding ancient landslide, and the value analysis of sliding zone parameters in different regions, it is determined that the blue strip area in Figure 11 is the tensile failure region. The red strip area is the shear failure region. And all the other green strip region is the undamaged region.

Due to the erosion effect caused by the variation of reservoir water level, the stage I sliding body strip 5 weight loss. Here, this paper regards strip 5 losing weight as the starting sliding force (572.31 kN/m). The residual sliding force calculation results of different strips and each sliding body are shown in Table 2.

5. DISCUSSION

Contrastive analysis of the improved transfer coefficient method and the traditional transfer coefficient method. For the T22 multistage sliding ancient landslide in Xiaowan Hydropower Station, the stability coefficient calculated by the improved transfer coefficient method is compared with the stability calculated by considering some factors' influence and considering

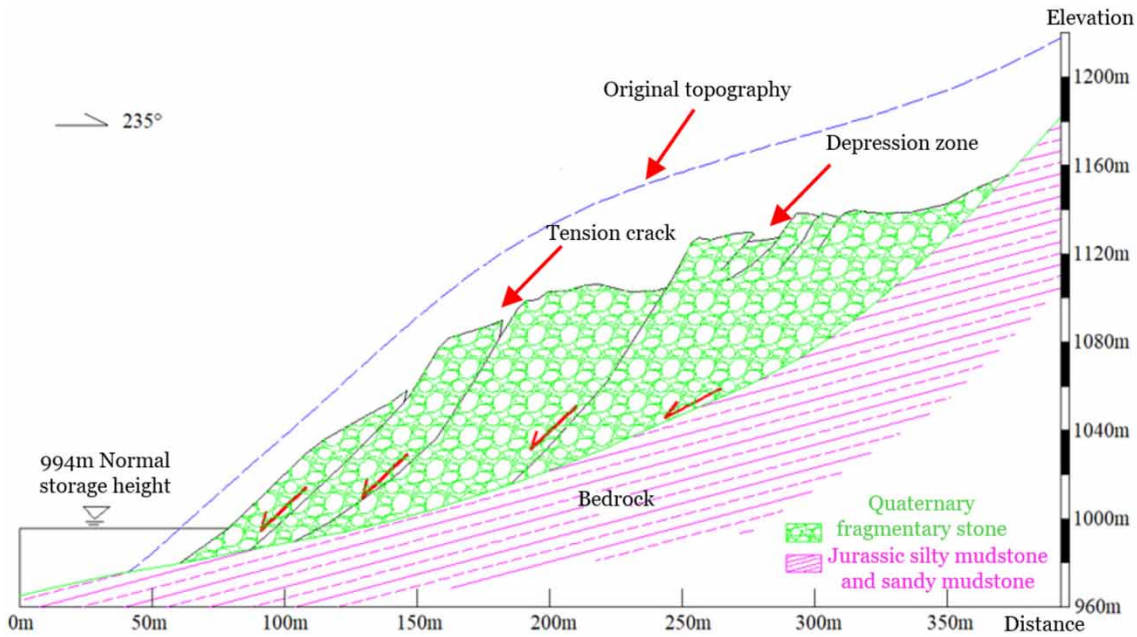

Figure 10 | T22 multistage sliding ancient landslide engineering geological profile.

Table 1 | Strength parameters values of T22 multistage sliding ancient landslide sliding zone soil in Xiaowan Hydropower Station

Sliding zone soil state	Cohesive (kPa)	Internal friction angle (°)
Peak intensity	16.8	15.3
Residual strength	13.4	12.9

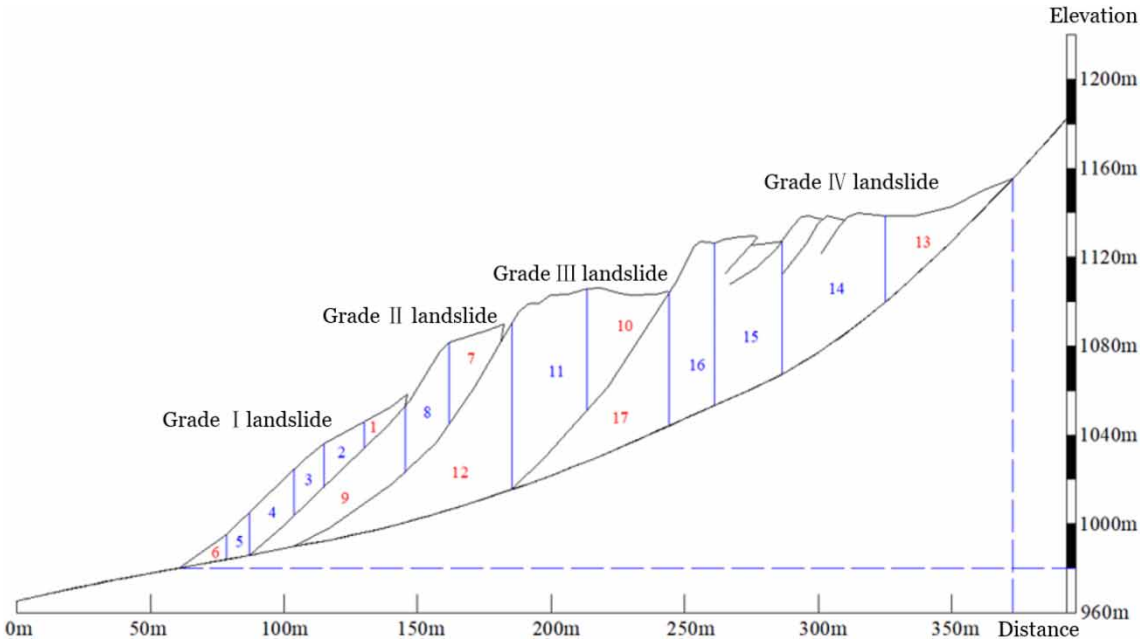

Figure 11 | Strip division and calculation model of T22 multistage sliding ancient landslide.

Table 2 | The T22 multistage sliding ancient landslide residual sliding force calculation results

Sliding body number	Strip number	W_i(kN · m^{-1})	α (°)	$\Delta\alpha$(°)	ψ_i	R_i(kN · m^{-1})	T_i(kN · m^{-1})	$\psi_i E_{i-1}$(kN · m^{-1})
Stage I sliding body	1	2,756.10	58	–	–	452.17	2,893.41	–
	2	3,982.14	24	34	0.67	1,265.41	1,231.57	2,269.74
	3	4,513.23	24	0	1.00	1,324.58	1,208.14	1,327.45
	4	4,257.58	21	3	0.97	1,107.21	1,154.63	887.41
	5	5,251.09	21	0	1.00	507.34	503.29	569.33
	6	6,217.33	18	3	1.00	632.74	585.11	742.56
Stage II sliding body	7	2,617.43	62	–	–	498.14	3,345.88	–
	8	4,327.55	47	15	0.82	1,352.29	2,473.19	2,852.16
	9	3,897.14	35	12	0.85	1,467.81	1,653.24	2,734.31
Stage III sliding body	10	2,634.59	42	–	–	789.31	587.14	–
	11	3,124.54	17	25	0.89	1,038.41	2,120.45	2,387.12
	12	2,706.28	17	0	1.00	821.03	774.58	952.13
Stage IV sliding body	13	2,434.12	54	–	–	358.12	1,853.26	–
	14	3,617.52	35	19	0.79	877.24	1,765.58	1,598.37
	15	3,858.43	35	0	1.00	1,045.31	1,533.71	1,675.14
	16	3,345.21	18	17	0.81	1,124.35	884.32	276.14
	17	2,321.47	18	0	1.00	705.21	573.13	1,731.25

none of the factors (Zhao *et al.* 2023). Considering the influence of some factors means that (1) the particle migration effect is not considered, that is, the stage I sliding body front edge exists in the multistage sliding body, and there is a key strip anti-sliding effect. (2) The differences of sliding zone soil parameters values are not considered, that is, the multistage sliding body strength parameters do not weaken gradually, and there is no difference in different sliding zone regions. (3) The interaction force between sliding bodies is not considered, that is, the multistage sliding body is regarded as a single independent sliding body, and there is no interaction influence between sliding bodies. At the same time, to compare the difference in landslide stability under the influence of different factors, this paper also calculates the stability coefficient when the whole landslide is unstable (Pacheco *et al.* 2023).

Table 3 | Comparison of T22 ancient landslide multistage sliding body stability coefficients in Xiaowan Hydropower Station under different calculation conditions

Sliding body number	Take all three factors into account	The particle migration effect is not considered	The sliding zone soil strength parameter value is not considered	The sliding bodies' interaction force is not considered	None of the three factors are considered	Overall sliding instability
Stage I sliding body	0.691	0.772	0.836	0.875	0.971	0.993
Stage II sliding body	0.763	0.831	0.881	0.913	0.932	
Stage III sliding body	0.738	0.864	0.932	0.951	0.914	
Stage IV sliding body	0.752	0.813	0.902	0.897	0.952	

According to the data analysis results in Table 3, when the three factors are not considered, the sliding bodies' stability coefficients from back to forward are increasing by 28.84, 18.13, 19.26, and 21.01%, respectively, than the improved transfer coefficient method calculating results. Compared with the improved transfer coefficient method calculating results are smaller than the stability coefficients calculating results when ancient landslide overall unstability. Therefore, we can think that the traditional transfer coefficient method may cause the deviation of ancient landslide stability evaluation, which does not reflect the actual landslide stability (Tong *et al.* 2021).

By comparing and analyzing the stability calculation results of the improved transfer coefficient method and considering the influence of some factors, we can see that the stability calculation results of the improved transfer coefficient method are the least. Because the improved transfer coefficient method takes into account the particle migration effect of the multistage sliding ancient landslide affected by reservoir water level variation, the interaction force between multistage sliding bodies, and the difference of sliding zone soil strength parameters, it can better reflect the progressive instability failure process of multistage sliding ancient landslide (Haeri *et al.* 2021; Wen *et al.* 2022).

Therefore, when evaluating the stability of multistage sliding ancient landslide under the combined action of reservoir level variation and rainfall, the stability calculation results of the improved transfer coefficient method should be adopted, which can ensure that the supporting structure can provide sufficient supporting force in the support design process and effectively complete the control of ancient landslide. In the improved transfer coefficient method, the sliding force is closely related to the cohesive force and internal friction Angle of the sliding body. The sliding force is only related to its gravity, which makes the settlement result of the stability coefficient small on the whole.

The accurate assessment of multistage sliding ancient landslides stability in hydropower station reservoir area still cannot ignore the impact of climate change. Further research will be needed in the evaluation of landslide stability within regional climate change, and suitable monitoring methods and machine learning methods (Shahid *et al.* 2018; Xu *et al.* 2019; Wang *et al.* 2020).

6. CONCLUSION

By improving the traditional transfer coefficient method, this manuscript accurately evaluates the stability of the multistage sliding ancient landslide in the reservoir area of Xiaowan Hydropower Station under the combined influence of reservoir level variation and rainfall and draws the following conclusions:

(1) The improved transfer coefficient method can accurately evaluate the sliding body stability of multistage sliding ancient landslides under the combined action of reservoir water level variation and rainfall. The improved transfer coefficient method stability coefficient calculation results are less than that of the traditional transfer coefficient method. Based on the stability coefficient calculated by the improved transfer coefficient method, the supporting force of the multistage sliding ancient landslide retaining structure will be greater.

(2) In the progressive failure process of a multistage sliding ancient landslide, the sliding body can be divided into a tensile failure zone, shear failure zone, and critical undamaged zone. The sliding body strength parameter in the tensile failure region is recommended to be zero. The sliding body strength parameters in the shear failure region are recommended to be residual strength. And the sliding body strength parameters in the critical unbroken region are recommended to be peak strength. The stability coefficient calculation result of multistage sliding ancient landslide by considering the sliding body region division will be more realistic. The interaction force between strips can also not be ignored.

(3) The improved transfer coefficient method takes into account the dynamic water pressure caused by the repeated reservoir water level rise and fall, the ancient landslide front erosion phenomenon due to the effect of particle migration, and the effect of hydrostatic pressure generated during rainfall infiltration, which is more consistent with the multistage sliding ancient landslides mechanical characteristics. By using the improved transfer coefficient method to analyze the T22 ancient landslide stability in Xiaowan Hydropower Station, it can be seen that the stability coefficient of the multistage sliding body shows a gradually increasing trend, that is, the sliding surface is gradually connected from front to back, which conforms to the typical multistage sliding characteristics.

FUNDING

This research was financially supported by the Chengdu University of Technology Postgraduate Innovative Cultivation Program: Study on red-bed soft rock trans-dimensional damage mechanical properties and constitutive model in central Yunnan under long-term soak (CDUT2022BJCX007).

DATA AVAILABILITY STATEMENT

All relevant data are included in the paper or its Supplementary Information.

CONFLICT OF INTEREST

The authors declare there is no conflict.

REFERENCES

Chen, L. L., Zhang, W. G., Zheng, Y., Gu, D. & Wang, L. 2020 Stability analysis and design charts for over-dip rock slope against bi-planar sliding. *Engineering Geology* **275**, 105–125.

Dolojan, N. L. J., Moriguchi, S. J., Hashimoto, M., Tinh, N. X., Tanaka, H. & Terada, K. 2023 Hydrologic-geotechnical modeling of shallow landslide and flood hazards caused by heavy rainfall. *Engineering Geology* **323**, 107–126.

Dou, H. Q., Xie, S. H., Wang, H. & Jian, W. B. 2023 Seepage characteristics and stability analysis of spherical weathered granite soil slope under rainfall conditions. *Journal of Engineering Geology* **31** (02), 638–649.

Guo, C. B., Ni, J. W., Yang, Z. H., Wu, R. A., Sun, W. F. & Zhang, Y. Y. 2021 Development characteristics and stability evaluation of large ancient landslide in the Luding Member of Dadu River, western Sichuan. *Geological Bulletin of China* **40** (12), 1981–1991.

Haeri, S. M., Akbari, G. A. & Kamali, Z. M. 2021 Unsaturated 3D column method: New method for evaluation of stability of unsaturated slopes subjected to vertical steady-state infiltration and evaporation. *International Journal of Geomechanics* **21** (10), 1943–1966.

He, M. & Zhao, Q. H. 2010 Improved transfer coefficient method based on directional angle correction. *Geological Hazard and Environmental Protection* **21** (01), 79–82.

He, S. J., Liu, J. R., Wu, S. R., Zhang, C. S. & Ye, S. Y. 2011 Research on three-dimensional stability simulation of multistage landslide in Xiayhe River. *Journal of Railway Engineering* **28** (11), 24–29.

Jiang, J. F., Zhao, Q. H., Jiang, H. H., Wu, Y. & Zheng, X. 2022 Stability evaluation of finite soil slope in front of piles in landslide with displacement-based method. *Landslides* **19** (11), 2653–2670.

John, B., Roger, M. & Delia, M. G. 2016 Reconstructing the recent failure chronology of a multistage landslide complex using cosmogenic isotope concentrations: St Catherine's Point, UK. *Geomorphology* **268**, 288–295.

Li, X. P., Chong, J. X., Lu, Y. B. & Li, Z. 2022 Application of information gain in the selection of factors for regional slope stability evaluation. *Bulletin of Engineering Geology and the Environment* **81** (11), 470.

Li, G., Tang, M. G., Zhang, M. L., Peng, D. L., Zhao, H. L. & Zhou, J. 2023 Slope stability under the influence of irrigation and frozen stagnant water effect in Heifangtai. *Bulletin of Engineering Geology and the Environment* **82** (7), 254.

Liao, Y., Le, J., Hu, L., Gu, W. W. & Xu, J. X. 2023 Based on Fredlund & Xing, seepage analysis of the model in the application of terraced fields in east Sichuan red layer landslide. *Hydrogeology Engineering Geology* **50** (03), 104–114.

Liu, T., Zhang, M., Wang, L. C., Yang, L. & Yin, B. G. 2023 Jiang top cliff ancient landslide formation evolution mechanism and deposit stability evaluation. *Geological Report of Science and Technology* 1–14.

Pacheco, Q. R., Velastegui, M. A., Montalván, B. N., Morante-Carballo, F., Korup, O. & Daleles Rennó, C. 2023 Land use and land cover as a conditioning factor in landslide susceptibility: A literature review. *Landslides* **20** (5), 967–982.

Ren, C. C. 2020 *Reservoir Operation Period Wading Bank-Slope Stability Coefficient Calculation of Transfer Coefficient Method to Improve*. Hefei University of Technology, Hefei, China.

Sarada, P. P. & Tariq, S. 2020 Stability assessment of landslide-prone road cut rock slopes in Himalayan terrain: A finite element method based approach. *Journal of Rock Mechanics and Geotechnical Engineering* **12** (1), 59–73.

Sepe, C., Calcaterra, D., Di, M. D., Fusco, F., Tufano, R., Vitale, E. & Guerriero, L. 2023 Triggering conditions and propagation of the December 2019 Palma Campania landslide: Implications for residual hazard estimation at recurrent landslide sites. *Engineering Geology* **322**, 107–122.

Shahid, M., Cong, Z. T. & Zhang, D. W. 2018 Understanding the impacts of climate change and human activities on streamflow: A case study of the Soan River basin, Pakistan. *Theoretical and Applied Climatology* **134** (1–2), 2127–2150.

Song, B. J., Cheng, Y. F., Yan, C. L., Han, Z., Ding, J., Li, Y. & Wei, J. 2019 Influences of hydrate decomposition on submarine landslide. *Landslides* **16** (11), 105–124.

Sun, Z. B., Huang, G. X., Hu, Y. N., Dias, D. & Ji, J. 2023 Reliability analysis of pile-reinforced slopes in width-limited failure mode considering three-dimensional spatial variation of soil strength. *Computers and Geotechnics* **161**, 105–124.

Tan, F. L., Hu, X. L., Zhang, Y. M., Xu, C. & Li, R. 2015 Pull-type landslide thrust calculation method research. *Rock and Soil Mechanics* **4** (S2), 532–538.

Tan, F. L., Hu, X. L., Zhang, Y. M., He, C. C. & Zhang, H. 2016 Different types of landslide stability and gradual failure process study. *Rock and Soil Mechanics* **5** (S2), 597–606.

Tong, D. F., Tan, F., Su, A. J., Song, H. B., Lu, Z. C. & Yu, C. 2021 Based on multi-source data Tan Jiawan landslide deformation mechanism and stability evaluation. *Journal of Geological Science Bulletin* **40** (4), 162–170.

Wang, X., Wang, S. & Qi, J. 2020 Open channel landslide hazard assessment based on AHP and fuzzy comprehensive evaluation. *Water Science & Technology Water Supply* **20** (8), 3687–3696.

Wang, C. T., Min, H., Zhu, T., Wang, H., Qin, W. & Zhang, G. 2022 Failure mechanism and stability analysis of the landslide: A case study for open pit iron mine in Xichang, Sichuan, China. *Natural Hazards* **116** (1), 663–691.

Wang, L. F., Xia, W. C., Ran, M., Zhang,, J. X. & Cheng, P. 2023 Considering reservoir water fluctuation and sliding zone weakening the role of bank slope and slide mechanism analysis. *Chinese Journal of Geological Hazard and Prevention and Control* (02), 30–41.

Wen, H., Chen, G. Q., Li, H., Ma, J. G. & Wu, Z. L. 2022 Improvement of transfer coefficient method with rainfall landslide sliding multistage study. *Journal of Geological Science and Technology* **9** (6), 162–168.

Wu, L. L., He, K. Q., Guo, L., Zhang, J., Sun, L. N. & Jia, Y. Y. 2022 Research on the excavation stability evaluation method of Chaqishan ancient landslide in China. *Engineering Failure Analysis* **141**, 106–135.

Xiao, R. H., Wang, S. J., He, X. H., Zhang, X. P., Rao, X. Y. & Luo, B. 2013 Multistage stability analysis method for heterogeneous slope. *Chinese Journal of Geotechnical Engineering* **35** (06), 1062–1068.

Xu, C. 2022 *Study on Evolution Model of Multi-Layer Slide-Resistant Pile System and Stress Characteristics of Anti-Slide Pile*. China University of Geosciences, Wuhan, China.

Xu, B. D. & Ma, J. 1979 Engineering geological analogy method for determining landslide thrust. *Hydrogeology Engineering Geology* **1** (01), 18–23.

Xu, B. D. & Wang, G. X. 1980 Research on landslide control. *China Railway Science* **1** (01), 110–122.

Xu, Q., Yang, H., Tang, M., Li, S. L., Li, H. J., Xiao, X. X., Alonso-Rodriguez, A. & Cai, G. J. 2019 Variability of permeability and seepage characteristics in soil landslides: A test case in the Three Gorges Reservoir Area, China. *Water Supply* **19** (8), 2453–2463.

Xue, Y., Miao, F. S., Wu, Y. P., Dias, D. & Li, L. 2023 Combing soil spatial variation and weakening of the groundwater fluctuation zone for the probabilistic stability analysis of a riverside landslide in the Three Gorges Reservoir area. *Landslides* **20** (5), 1013–1029.

Yang, D. F., Hu, X. L., Xu, C., Wang, Q., Niu, L. F. & Zhang, J. H. 2022 Based on physical model test of multilayer sliding zone of landslide deformation evolution characteristics. *Journal of Geological Science and Technology* **9** (02), 300–308.

Yang, Y. T., Dai, Z. W., Lu, Y. S., Zhang, C. Y., Yan, H., Hou, X. F. & Tang, J. G. 2023 Bank of the ancient landslide deformation characteristics and the double sliding stability response. *Earth Science* 1–15.

Yi, W., Wei, Z. H., Huang, X. H. & Lei, D. X. 2023 *Study on Rainfall Threshold and Early Warning Model of Rainfall-Type Accumulation Landslide: A Case Study of Wangjiapo Landslide*. Three Gorges University (Natural Science Edition) **45** (06), 36–43.

Zhang, Y. B. 2019 *Study on Optimization of Slope Cutting and Load Reduction Scheme of Typical Thick Landslide in Three Gorges Reservoir Area*. Hefei University of Technology, Hefei, China.

Zhang, X. X., Fan, X. M., Wang, W. S., Guo, J. S., Du, S. L. & Yu, Z. Y. 2023a High altitude wedge starting mechanism of landslide centrifugal model test study. *Journal of Rock Mechanics and Engineering* **42** (05), 1202–1213.

Zhang, Q., Ju, N. P., Zhang, C. Q., Zhang, J. J., Ke, H. & Liu, H. 2023b Deformation mechanism of steep soft bedding rock landslide when reservoir water level changes. *Journal of Chengdu University of Technology (Natural Science Edition)* **50** (02), 206–217.

Zhang, Y. J., Zhang, X., Nguyen, H., Li, X. & Wang, L. 2023c An implicit 3D nodal integration based PFEM (N-PFEM) of natural temporal stability for dynamic analysis of granular flow and landslide problems. *Computers and Geotechnics* **159**, 105–123.

Zhao, Z., Chen, J. H., Yao, J. M., Xu, K., Liao, Y., Xie, H. & Gan, X. 2023 An improved spatial case-based reasoning considering multiple spatial drivers of geographic events and its application in landslide susceptibility mapping. *Catena* **223**, 106–119.

First received 28 November 2023; accepted in revised form 9 February 2024. Available online 5 March 2024